Research on
Engineering
Structures & Materials
journal homepage: http://jresm.org

RESEARCH GROUP

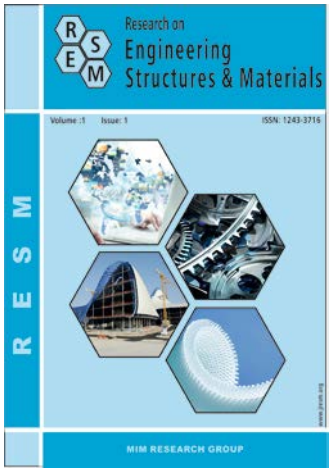

Pristine and coated $LiNi_{1/3}Mn_{1/3}Co_{1/3}O_2$ as positive electrode materials for li-ion batteries

Ahmed. M. Hashem*, Rasha. S. El-Tawil, Mohamed Abutabl, Ali. E. Eid

Online Publication Date: 3 June 2015
URL: http://www.jresm.org/archive/resm2015.07en0315
DOI: http://dx.doi.org/10.17515/resm2015.07en0315

Journal Abbreviation: *Res. Eng. Struct. Mat.*

To cite this article
Hashem AM, El-Tawil RS, Abutabl M, Eid AE. Pristine and coated $LiNi_{1/3}Mn_{1/3}Co_{1/3}O_2$ as positive electrode materials for li-ion batteries. *Res. Eng. Struct. Mat*., 2015; 1: 81-97.

Research on
Engineering
Structures & Materials
journal homepage: http://jresm.org

RESEARCH
GROUP

Research Article

Pristine and coated $LiNi_{1/3}Mn_{1/3}Co_{1/3}O_2$ as positive electrode materials for li-ion batteries

Ahmed. M. Hashem[1*], Rasha. S. El-Tawil[1], Mohamed Abutabl[2], Ali. E. Eid[1]

[1]*National Research Centre, Inorganic Chemistry Department, Egypt*
[2]*Cairo University, Department of Physical Chemistry, Egypt*

Article Info

Article history:
Received 15 Mar 2015
Revised 24 May 2015
Accepted 25 May 2015

Keywords:
$LiNi_{1/3}Mn_{1/3}Co_{1/3}O_2$
Co-precipitation
Li-ion batteries
Surface modification
^{7}LiMAS NMR

Abstract

Layered $LiNi_{1/3}Mn_{1/3}Co_{1/3}O_2$ (NMC) positive materials were synthesized by efficient, low cost and easy manageable methods such as oxalate co-precipitation and sol-gel processes. Preliminary electrochemical results show that sol-gel sample provide better results than co-precipitated samples. With the aim to improve the properties of the co-precipitated samples these were coated with carbon and alumina bearing in mind the co-precipitated method is suitable for large scale production. The subsequently performed local structure investigations revealed well crystallized layered cathode materials with α-$NaFeO_2$-type structure (R-3m space group). Sample tests using both the scanning electron microscope (SEM) and the transmission electron microscope (TEM) showed submicron particles with a slight tendency to agglomerate and furthermore the existence of a thin film that encapsulates the oxide particles. 7Li magic angle spinning nuclear magnetic resonance (7LiMAS NMR) measurements were carried out for pristine and coated samples to compare the cation arrangement in the transition metal layers. Finally, electrochemical tests revealed a remarkable improvement in capacity retention of the coated oxides compared to the parent compounds.

1. Introduction

Since the last decade, lithium secondary batteries have received much attention due to their potential use in large-scale applications such as plug-in hybrid electric vehicles (PHEV) and stationary storage systems. For these large-scale applications, high energy density, long-term cycling performance, better tolerance in harsh conditions, and economically viable synthesis are important factors. The $LiCoO_2$//graphite electrochemical cells, which are successfully used in small-scale portable electronics, often fail to meet these requirements. Therefore, there are still considerable efforts underway to develop more reliable, inexpensive and safe active materials for the large-scale lithium secondary battery applications [1]. Since the cathode material $LiNi_{1/3}Mn_{1/3}Co_{1/3}O_2$has been synthesized by Ohzuku and Makimura [2], it attracts a lot of attentions due to its lower cost, lower toxicity and higher capacity, which are superior to those of the individual layered compounds, $LiMO_2$ (M = Co, Ni, or Mn) [3]. Typical compositions that have been investigated include $LiNi_{0.8}Co_{0.2}O_2$ [4], $LiCo_{0.5}Ni_{0.5}O_2$ [5], $LiCo_{0.8}Mn_{0.2}O_2$

*Corresponding author: ahmedh24@hotmail.com
DOI: http://dx.doi.org/10.17515/resm2015.07en0315
Res. Eng. Struct. Mat. Vol.1 Iss.2 (2015) 81-97

[6], $LiNi_xCo_{1-2x}Mn_xO_2$ [7] and $LiNi_{0.6}Co_{0.4-x}Mn_xO_2$ [8]. $LiNi_{1/3}Mn_{1/3}Co_{1/3}O_2$possesses high specific capacity of about ~160 mAhg−1 in the voltage range 2.5–4.4 V and mild thermal behaviour at charged state. In addition, the high power pulse capability and the accelerated aging test of $C/LiNi_{1/3}Mn_{1/3}Co_{1/3}O_2$ cells have shown that $LiNi_{1/3}Mn_{1/3}Co_{1/3}O_2$ is more suitable for lithium-ion batteries in HEV applications [9]. It has been established that under normal conditions of charging and discharging, Mn in $LiNi_{1/3}Co_{1/3}Mn_{1/3}O_2$ exists in +4 oxidation state, thus avoiding Jahn–Teller effect which induces structural distortion in the compound. However, although NMC material exhibits an excellent performance as mentioned above, it has some drawbacks to overcome such as low tap density and relatively poor cycling stability. These drawbacks impede the industrialization process of this material. Several measures were investigated to improve the cycle-ability of NMC, such as exploring new synthesis methods, doping with small amounts of aliovalent ions, coatings of various substances, etc. Surface encapsulation is a particularly effective approach to enhance the cycling stability. Although the reason for the improvement of the cycle-ability is not completely understood, this technology is still widely applied [10-11]. NMC material is currently prepared by solid-state reaction or by hydroxide co-precipitation synthesis method. The solid-state reaction method often results in an impure and inhomogeneous product with inferior electrochemical performance. One possibility to achieve better materials is the use of the hydroxide co-precipitation method, in which a homogeneous precursor such as $[Ni_{1/3}Mn_{1/3}Co_{1/3}](OH)_2$ is prepared [12]. The synthesis of NMC by sol–gel method using different chelating agents, e.g. citric acid and polymers, is also reported [13–15]. In order to enhance the electrochemical performance of NMC, several efforts have been made to study the surface modification of particles. Sinh et al.[14] prepared carbon coated NMC by an inverse micro-emulsion route with glucose. Charge–discharge tests showed that carbon coating on the NMC particles enhances the discharge capacity. For a sample, 0.3 wt. % carbon coating provides capacity of 158 mAh g-1, which is higher than that of the bare sample (135 mAh g-1). Furthermore, it was reported that carbon coating on particles is effective not only in enhancing the conductivity between particles but also in protecting the particles from chemical attack from the electrolyte [15]. Hashem et al. [16] used an oxalate co-precipitation method for the synthesis of NMC and modified the surface layer of the NMC particles by mixing them with sucrose and starch. Further studies showed that a variety of films deposited on the surface of NMC, such as CeO_2 [17], TiO_2 [18], Al_2O_3 [19], ZrO_2 [20]and Ag [21], improve the electrochemical properties as well. The formation of such an inorganic passivation layer provides a two-fold benefit in that it reduces disproportion/dissolution reactions and also minimizes electrolyte decomposition on the surface of the electrode material. Al2O3 appears to be the most popular protective surface coating due to the high abundance of aluminium, the low material cost and the ease of film deposition. Alumina was successfully applied on different positive electrode materials such as $LiCoO_2$, $LiMnO_2$, and NMC [22]. Myung et al. speculated that Al2O3 might act as a “scavenger” of F− ions through the formation of Al–O–F and Al–F layers, thus limiting the concentration of harmful HF species [23]. With the aim to shorten the process time and possibly reduce the synthesis cost, two synthesis procedures for NMC powders are presented in this paper, i.e. co-precipitation and sol–gel methods. Samples are characterized by X-ray diffraction (XRD), scanning electron microscope (SEM), transmission electron microscope (TEM) and ^7Li magic angle spinning nuclear magnetic resonance (^7Li MAS-NMR) measurements. As the co-precipitation method seems to be more suitable for large scale production, further surface modification by alumina and carbon coating are carried out onto NMC particles to improve their electrochemical properties. A remarkable electrochemical improvement has been observed for both of alumina and carbon coatings. The structure, morphology and electrochemical performances of all prepared samples are compared and discussed in detail.

2. Material and Method

2.1 Preparation of Samples

$LiNi_{1/3}Mn_{1/3}Co_{1/3}O_2$ samples were prepared using two wet-chemistry methods, i.e. sol–gel (named 333SG) and co-precipitation (named 333CP) method. Furthermore, surface modification was carried out on sample 333CP by alumina and carbon coating. These samples are named hereafter (333Al) and (333C), respectively

Sol-gel powders (333SG) were synthesized using citric acid as a chelating agent. Stoichiometric amounts of $Li(CH_3COO)\bullet 2H_2O$, $Mn(CH_3COO)_2\bullet 4H_2O$, $Ni(CH_3COO)_2\bullet 4H_2O$, and $Co(CH_3COO)_2\bullet 4H_2O$ (molar ratio Ni/Co/Mn = 1:1:1) were dissolved in distilled water. The solution was added drop-wise to a continuously stirred aqueous solution of 1 mole citric acid. The pH value was adjusted to 7.0-8.0 with ammonium hydroxide and the solution was then heated to 70–80°C, while stirring to evaporate the organic solvents until a transparent sol was obtained. The resulting gel precursor was calcined at 450°C for 8 h in air to remove the organic contents. Finally, the powder was grinded in a mortar and air calcined at 900 ºC for 12 hours

Co-precipitation powders (333CP) were synthesized using oxalic acid as precipitating agent. Stoichiometric amounts of $Ni(NO_3)_2\bullet 6H_2O$, $Co(NO_3)_2\bullet 6H_2O$ and $Mn(NO_3)_2\bullet 4H_2O$ (molar ratio of Ni/Co/Mn = 1:1:1) were dissolved in distilled water. The solution was added drop-wise to 100 ml 1M oxalic acid while stirring till complete precipitation of the oxalate precursor. The precipitated precursor was filtered and dried at 100 °C for 12 hours. A stoichiometric amount of $LiOH\bullet H_2O$ was mixed thoroughly with the dried powder and calcined at 900°C for 12 hours in air to obtain the final product. These powders were further treated to obtain coated samples as outlined below.

A part of 333CP Particles was coated with alumina (sample 333Al) using an appropriate amount of aluminum nitrate mixed with the 333CP sample to obtain 2% alumina coating. An ethanol solution as dispersing medium was utilized to obtain a homogenous mixture. The solution was stirred for 1 h and then gently heated at 40-50 ºC until complete evaporation of the ethanol. The final product was obtained by calcination at 450 ºC for one hour in air.

The carbon coated (333C) particles were prepared by a careful mixing of the 333CP sample with a required amount of glucose in an agate mortar, then stirring with ethanol for one hour followed by evaporation of the ethanol during stirring at 50-60°C. After complete evaporation, the dried mixture was calcined at 500 °C for one hour in air.

2.2 Characterization of Samples

The crystal structure was analyzed by XRD using a Philips X'Pert apparatus equipped with a CuKα X-ray source (λ=1.5406 Å). XRD measurements were collected in the 2θ range 10-80°. FTIR spectra were recorded with a Bruker IFS 113 vacuum interferometer. In the far-infrared region (400–100 cm^{-1}), the vacuum bench apparatus was equipped with a 3.5-μm-thick Mylar beam splitter, a glow-bar source, and a DTGS/PE far-infrared detector. Raman spectra were measured using a Micro-Raman-Laser spectrometer Lab-Ram (Horiba-Jobin-Yvon) with a microscope lens (×50), a filter D2, diaphragm (400 μm) and 150 μm slit. The spectra were recorded using the laser excitation line at 632 nm. Sample morphology was observed by using SEM and TEM (TEM: JEOL, JEM-1230, Japan). The chemical composition of the synthesized samples was analyzed by EDX. The ^7Li magic-angle spinning (MAS) NMR measurements were performed on a Bruker Avance 200 MHz spectrometer (B_0 = 4.7 T) using 1.3 mm zirconia rotors in a dry nitrogen atmosphere. An aqueous 1M LiCl solution served as reference material for the chemical shift of ^7Li (0 ppm). The ^7Li MAS NMR spectra were recorded at room temperature at a spinning speed of about

60 kHz with a rotor synchronized Hahn-echo sequence (π/2–τ – π – τ – acquisition). Typical values for the recycle delay and the π /2 pulse lengths were 1 s and 2 μs, respectively.

Electrochemical tests were performed at room temperature in coin-type cells with a Li^+ metal foil as a counter electrode. The positive electrode was a mixture of 80 wt.% active material, 10 wt.% carbon black as a conductive agent and 10 wt.% polyvinylidenedifluoride (PVDF) as binder. 1 mol. L^{-1} $LiPF_6$ in EC:DMC (1:1) was used as electrolyte and the separator was a microporous polypropylene/polyethylene foil (Celgard 2325). The data was recorded with a Biologic battery cycler at different current densities in the potential range 2.5-4.3 V *vs*. Li^0/Li^+.

3. Results and Discussions

Four $LiNi_{1/3}Mn_{1/3}Co_{1/3}O_2$ samples were thoroughly analyzed: Two of them are the parent compounds synthesized by sol-gel (333SG) and by co-precipitation (333CP) method. The latter sample synthesized by co-precipitation was afterwards coated with Al2O3 (333Al) and carbon (333C). The XRD patterns of these NMC samples are shown in Figure 1. Results reveal the distinct well-defined peaks of the layered structure, which can be indexed on the basis of α-$NaFeO_2$ hexagonal structure (R3m space group). In this structure Li ions occupy the 3a site, Ni, Mn and Co are located on the 3b site, and O is located on the 6c site.

No obvious changes, such as the appearance of impurity peaks or significant peak shifts, are observed after coating NMC with carbon and Al_2O_3. The splitting of the (006)/(012) and (018)/110) doublets reveal the layered α-$NaFeO_2$ structure was formed [24]. These structural features are maintained after coating for samples calcined at 900ºC.

Rietveld refinements of XRD patterns were performed; the refined parameters are summarized in Table 1. It is shown that the cation mixing, i.e.. the interchange of lithium and nickel ions of the 3*a* and 3b sites, respectively, is clearly identified, as it is known to occur for the Ni-containing materials [25–28]. Results show a low degree of cation mixing of around 2 % for all NMC samples. The lattice parameters of pure and coated NMC powders are in good agreement with the values reported in the literature [2, 29]. Moreover, it is obviously seen that the bulk structure is not affected by the coating processes. These results implied that the coated films did not diffuse into the core of the particles. Thus the intrinsic electronic properties of the NMC particles do not change but the coating ensure a good electrical contact between them.

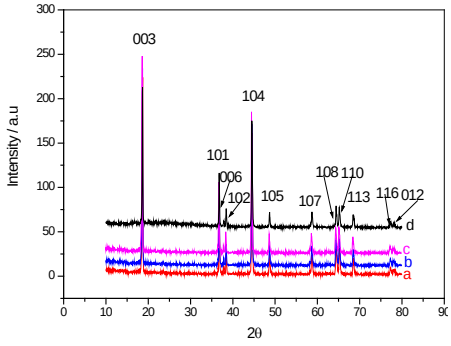

Fig.1. XRD patterns of NMC samples (a) 333CP, (b) 333Al, (c) 333C and (d) 333SG and the reflections indexed on the basis of the R $\overline{3}$ m space group

Table 1Structural parameters of NMC samples obtained from Rietveld refinements

Sample	a (Å)	c (Å)	z_0 (a.u.)	cationic mixing (%)
333SG	2.8570(4)	14.2178(45)	0.2555(28)	3.45(8)
333CP	2.8568(2)	14.2184(20)	0.2573(13)	1.95(2)
333Al	2.8570(2)	14.2196(25)	0.2574(15)	2.26(3)
333C	2.8570(3)	14.2188(31)	0.2571(18)	2.44(4)

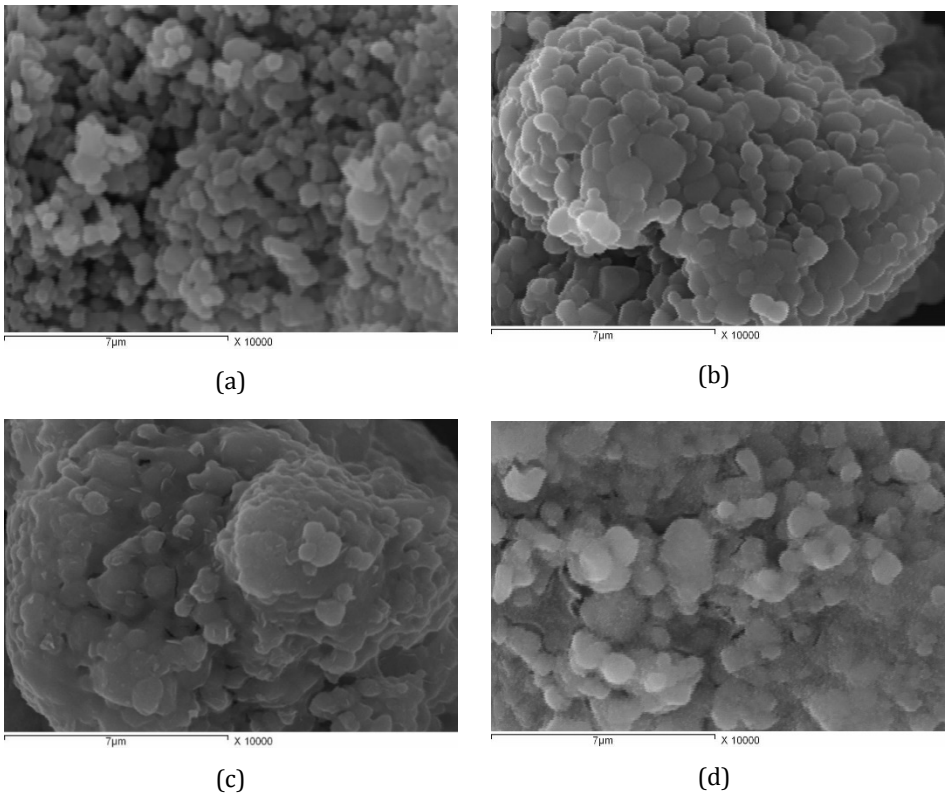

(a) (b)

(c) (d)

Fig.2. SEM images of the NMC samples (a) 333SG, (b) 333CP, (c) 333Al, and (d)333C

Figure 2(a-d) show the SEM images of NMC prepared samples. The synthesized powders consisted of distinct particles indicating a good crystallinity with a spherical-like shape. The agglomeration of particles prepared by co-precipitation seems to be bigger compared to the sol-gel agglomerates. Nevertheless, the particle size of the primary particles seems to be similar for all samples. EDX analysis of the 333Al sample confirmed the existence of Al due to the Al_2O_3 coating.

The particle morphology was studied in more detail by TEM As shown in Figures 3- 4. The TEM images show that the particle size of all prepared NMC powders are in the nanometric scale in the range 70-100 nm. These particles consist of well-dispersed monocrystallites, which are slightly agglomerated and show a small quantity of fragments. The samples

occur to be a mixture of spherical and elongated particles. Similar features were observed at any part of these samples, which appear to be highly homogeneous considering the area investigated. Figures 4(a – b) display clearly the presence of an amorphous-like layer with a thickness in the range of 2-10 nm covering the NMC particles. This surface layer appears as a grayish region at the edge of the NMC crystallites, while the core of the primary particle is observed as a dark region. It seems that the nature, the shape and the thickness of the coating layer depend on the coating substance. It is expected that the coating surrounding the particles would facilitate the lithium ion transfer and decrease the polarization of the electrode [30, 31].

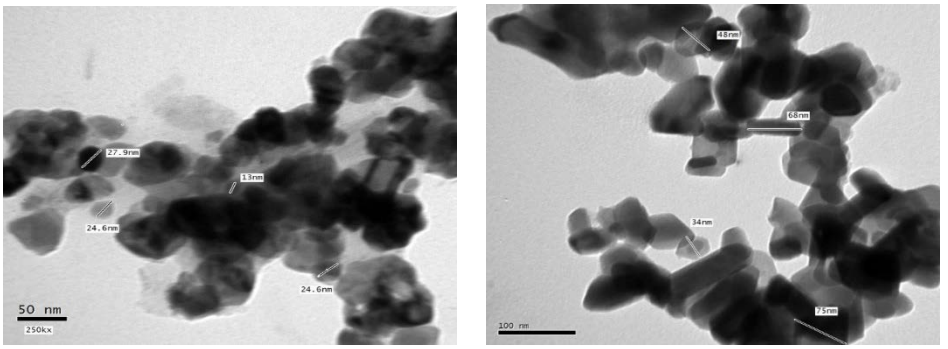

(a) (b)

Fig. 3. TEM images of the uncoated LNM samples (a) 333SG and (b) 333CP

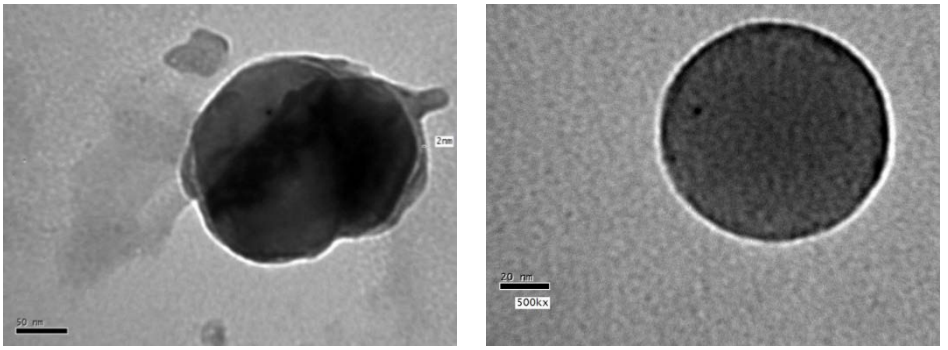

(a) (b)

Fig. 4. TEM images of the coated NMC samples (a) 333Al and (b) 333C

Figures 5 - 6 show the FTIR and Raman spectra of 333SG, 333CP, 333Al, and 333C samples, respectively, We observed that the characteristic bands of (Ni, Mn, Co)O_6 and LiO_6 octahedral entities of the NMC lattice are well resolved. Considering the space group R3m of α-$NaFeO_2$ hexagonal structure, i.e. $D^5{}_{3d}$ spectroscopic symmetry, the group factor theory provides the vibrational active modes represented as follows:

$$\Gamma = 3A_{1g} + 3E_g + 4A_{2u} + 3E_u \quad (1)$$

in which A_{1g} and $E_g$modes are Raman-active and A_{2u} and E_u modes are infrared active modes[32]. The A_{1g} and A_{2u} modes originate from the M–O symmetrical stretching, while E_g and E_u stem from the O–M–O bending vibrations [33]. Because of the D_{3d} site group of

the Wyckoff 3*b* site for the lithium ions, the Li cage mode is only infrared active. Since the compound has three transition-metal ions, we expect $3A_{1g}$ modes and $3E_g$ modes that overlap to give rise to the two broad A_{1g} and E_g bands. The E_g bands are centered at 475, 482, and 516 cm^{-1} and the A_{1g} bands are centered at 576, 602, and 639 cm^{-1} for M=Ni, Co, and Mn, respectively. These positions compare well with the corresponding bands of $LiNiO_2$, $LiCoO_2$, and λ-$LiMn_2O_4$, respectively. The position of the modes depends on the nature of the transition-metal ions (mass, ionic radius, oxidation state). The FTIR absorption spectrum of NMC is presented in Fig. 5. According to group factor analysis, the IR absorption bands are observed in three distinct regions. The lower-wave-number band at 230-250 cm^{-1} is attributed to the Li cage mode. The medium-wave-number region 400–520 cm^{-1} corresponds to the O–M–O asymmetric bending modes, while above 520 cm^{-1} the IR modes are due to the asymmetric stretching modes of the MO_6 octahedra. The frequency position of these modes depends on the nature of the transition-metal ions (mass, ionic radius, oxidation state) [34]. The band situated at 235 cm^{-1} is assigned to an asymmetric stretching vibration of the Li^+ ion with O^{2-} near neighbors in NMC. The medium frequency absorption bands at ca. 670, 616 and 525 cm^{-1} are attributed to the asymmetric stretching modes of MO_6 groups, whereas the low-frequency band at ca.478 and 380 cm^{-1} is assigned to the bending modes of O-M-O chemical bonds. The change in IR spectra due to metal oxides surface coating is identical to that recorded by [35]. Characteristic bands of $LiNi_{1/3}Mn_{1/3}Co_{1/3}O_2$ related to the position of LiO_6 and MO_6 were observed for the coated oxides. This means that the local structure does not noticeably change. In the coated oxides the characteristic bands are well resolved in comparison with the parent NMC. The FTIR characterization supports the results obtained by XRD that coating by metal oxide and carbon altered only the surface chemistry but the local structure inside the particles remains constant.

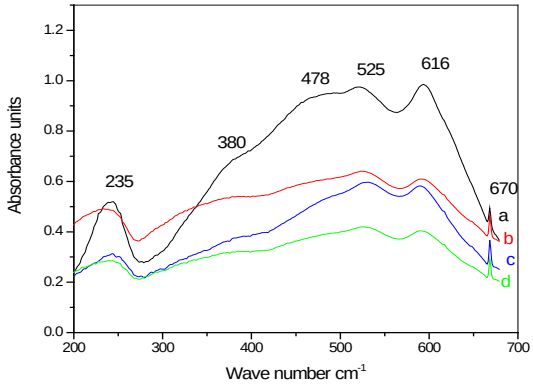

Fig. 5. FTIR spectra of NMC samples (a) 333SG, (b)333CP, (c)333Al, and (d)333C

Solid-state NMR provides a probe for the local environment of lithium ions [36–39]. It is well known that paramagnetic ions in the vicinity of lithium ions have strong effects on the NMR spectra due to the Fermi-contact mechanism, i.e. the transfer of spin density from the unpaired electrons of the paramagnetic ions to the lithium nucleus. Thus, the value of the resulting hyperfine shift depends on the specific local environment [39]. In the NMC framework, Co^{3+} is diamagnetic, but both Ni^{2+} and Mn^{4+} contribute to the hyperfine shifts [26-27]. Figure 7 shows the ^7Li MAS NMR spectra of the parent and coated NMC samples. Two strong contributions are discernible in these spectra. A rather narrow resonance is located at around 0 ppm and a group of resonances with large chemical shifts is covering the range from 0 to 1000 ppm. The broad contribution is identical for the sample prepared by co-precipitation, while it appears with a significantly lower intensity in the range up to

about 500 ppm for the sol-gel sample. The amplitude of the 0-ppm peak is sample specific: the uncoated NMC samples show the smallest 0-ppm peak, the sample coated with alumina shows the highest 0-ppm peak.

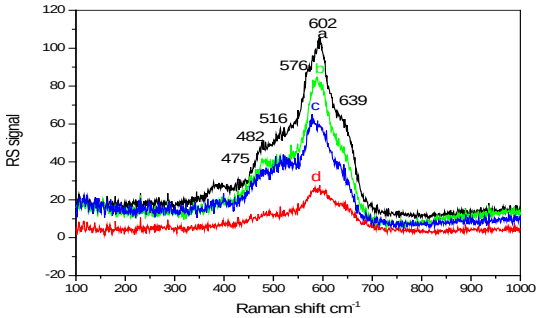

Fig. 6. Raman spectra of NMC samples (a) 333SG, (b)333CP, (c)333Al, and (d)333C

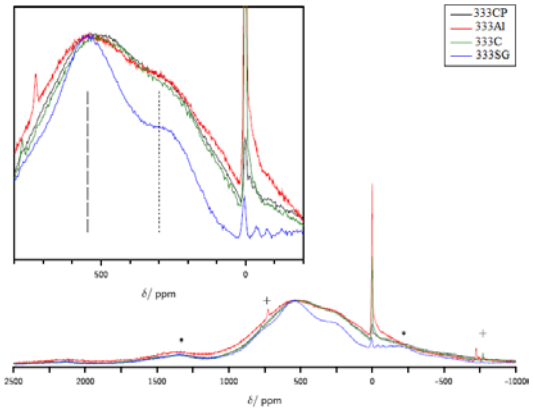

Fig. 7. 7Li Hahn-echo MAS NMR spectra of investigated samples acquired at ≈ 60 kHz spinning speed. The star (*) denotes the sidebands of the peak at ≈ 550 ppm and the cross (+) denotes the sidebands of the peak at ≈ 0 ppm. The inset shows a magnification of the -200-800 ppm range, where the lines mark spectral contributions due to different local environments of the Li ion. All spectra are normalized with respect to the maximum amplitude of the broad spectral contribution at ≈ 550 ppm

NMR spectra were analyzed by spectral deconvolution as shown in Figure. 8. The deconvolution reveals three major resonances in parent NMC samples: 755, 579, and 313 ppm in 333CP and 780, 561, and 279 ppm in 333SG (cf. Table 2). Whereas for 333CP the intensity of the resonances (including their relevant sidebands) decreases with increasing chemical shift, the intermediate resonance at 561 ppm has the highest intensity for 333SG. In both samples the significant smallest spectral contribution is provided by the resonance with the strongest shift. The local environment of the lithium nuclei that gives rise to the three major resonances and the narrow resonance at 0 ppm will be discussed as follows.

Previous 6Li MAS NMR and neutron scattering studies have shown that lithium can be found in two different sites of the NMC structure. The majority of Li^+ ions is present in the

interlayers, while a small percentage of lithium atoms is located in the intralayers because the Li^+ ions exchange easily with Ni^{2+}cations due to their similar ionic radius [27,28]. NMR is a quantitative method, therefore the strongest spectral contribution should stem from lithium in the interlayer space.

Using ^{6}Li NMR, Cahill et al.[27]determined three resonances in the range from 200 to 800 ppm and assigned these peaks to lithium ions in the interlayer space with different transition-metal distribution in the first cation coordination shell [37]. Adopting these results, we adopt the same interpretation for the three major resonances identified in the deconvolution of the 333CP and 333SG spectra. The observed hyperfine shifts can be readily explained by the three different local environments proposed by Cahill et.al. [27] (cf. Table 2). The asymmetric intensity distribution among the peaks might hint at partial clustering of Ni and Mn ions [28]. The degree of cationic disorder, i. e. the degree of exchange of Ni ions and Li ions, was already quantified by 6Li NMR on different samples [28]. The 7Li NMR spectra of the samples investigated here do not allow the identification of a resonance from the intralayer. In general, the resolution of ^{7}Li spectra is lower compared with ^{6}Li spectra [39]. Furthermore, the sidebands of the broad major resonances in our spectra obscure any additional small signals, in particular at larger shifts where contributions from lithium ions in the intralayer sites [26,27] could be expected. The value of 64 % for the 2/2/2 environment determined for the 333SG sample is higher than the value for the 333CP sample (31 %), as shown in Table 2. Since the 2/2/2 environment represents the configuration expected for a completely random distribution of cations, one can conclude that the transition metal ions are clustering less in the 333SG sample than in the 333CP sample or, in the other way around, are more randomly distributed.

Table 2 Deconvolution of the spectra of the 333CP and 333SG NMC samples. Calculated areas include all significant sideband contributions. Local coordination environments are assigned according to Cahill et al.[27]

sample	chemicalshift (ppm)	area/total area (%)	number of next nearest neighbors $Ni^{2+}/Co^{3+}/Mn^{4+}$
333CP	755	3	3/0/3
	579	31	2/2/2
	313	66	1/4/1
333SG	780	5	3/0/3
	561	64	2/2/2
	279	31	1/4/1

Using ^{7}Li MAS NMR, Menetrier et al. studied $LiNi_{0.425}Mn_{0.425}Co_{0.15}O_2$ prepared by co-precipitation method [40]. The resulting spectrum can be well compared with our data. A broad contribution stems from different local environments causing strong Fermi-contact shifts. The rather sharp signal close to 0 ppm is explained by traces of Li_2CO_3, which are commonly observed due to slight lithium excess in the synthesis. The XPS investigation of $LiNi_{0.4}Mn_{0.4}Co_{0.2}O_2$ revealed small amounts of LiOH, Li-oxide and Li-carbonate groups on the electrode surface prior to cycling [41]. Dupré et al. [42] pointed out that NMR study of $Li_{0.5}Ni_{0.5}Mn_{0.5}O_2$ displayed further diamagnetic impurities coming from the decomposition of the battery electrolyte contributing to the 0 ppm signal. The small shift of the diamagnetic signal requires a certain local separation of paramagnetic transition metals and diamagnetic lithium species. This effect could either be caused by a segregation of paramagnetic and diamagnetic compoundsor by the formation of a diamagnetic surface

layer of sufficient thickness on the paramagnetic particles. In the second case, an increase of thickness leads to a sharper NMR signal [42]. Therefore it can be concluded that the small peaks at 0 ppm observed in uncoated 333CP and 333SG reflect the thin layers of diamagnetic compounds in these samples, e.g. Li_2CO_3, while the increase of peak intensity in the coated samples indicates the increase of material which contains diamagnetic lithium and surrounds the paramagnetic phase. The maximum diamagnetic peak intensity obtained in 333Al is presumably enlarged by additional contributions from Li-Al-O compounds. This means that not only a pure Al_2O_3 phase is present, but also an intermixing with Lithium takes place.

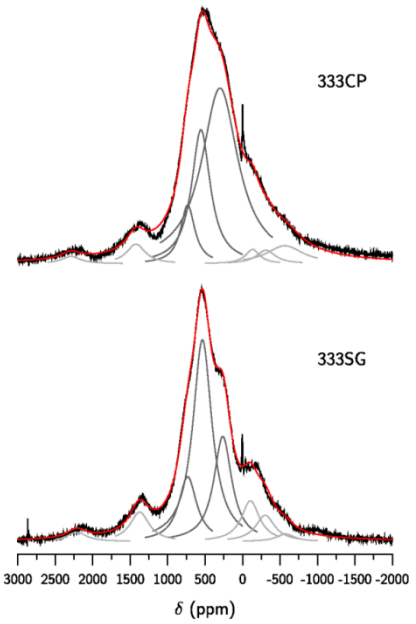

Fig.8.^{7}Li Hahn-echo MAS-NMR spectra of the as prepared 333CP (top) and 333SG (bottom) NMC samples. The experimental data (black line) is presented with its corresponding deconvolution. The sum of the deconvolution is shown by the red line, while the main peaks are given in dark grey and the major sideband contributions are displayed in light grey.

To investigate the electrochemical properties of NMC as positive electrode material in lithium-ion batteries, cyclic voltammetry (CV) measurements were carried out. Typical results are presented in Figures (9a-d), which show the cyclic voltammograms of samples 333SG, 333CP, 333Al and 333C, respectively, for five cycles performed at scan rate of 0.05 mVs-1. Redox reactions occur in the potential range 3.6-3.8V. An anodic peak is located at c.a. 3.8V, whereas a cathodic peak is located at c.a. 3.6 V. The voltage difference between anodic and cathodic peaks reduced after the first cycle due to the phenomenon called “electrode formation” which is the electrolyte wettability in the pores of the electrode. In fact it is a surface effect that disappeared at the second cycle[43].

This behavior is almost similar to the features of voltammograms of NMC reported by Chernova et al. [43]. It is well established that only Ni2+ and Co3+ ions are electrochemically active, while Mn with oxidation state 4+ is inactive [14]. The redox peaks in these figures are only attributed to the redox transitions of Ni2+/Ni3+ and Ni^{3+}/Ni^{4+} because the Co^{3+}/Co^{4+} redox reaction is expected to appear at potential above 4.6V in NMC. Note that the oxidation peak is observed at 4.2 V in LiCoO2 [44]. As the upper limit of the potential is maintained at 4.3V in the present study, only Ni2+/Ni4+ redox peaks are observed by the CV measurements. Almost the same redox peaks are observed for coated NMC electrodes; thus, we can conclude that the coating does not alter the NMC structure. The coating only prevents the electrodes from reacting with the electrolyte [19]. It is well known that the reaction at the interface induces an increase in the impedance and causes capacity fading of the cathode [45].

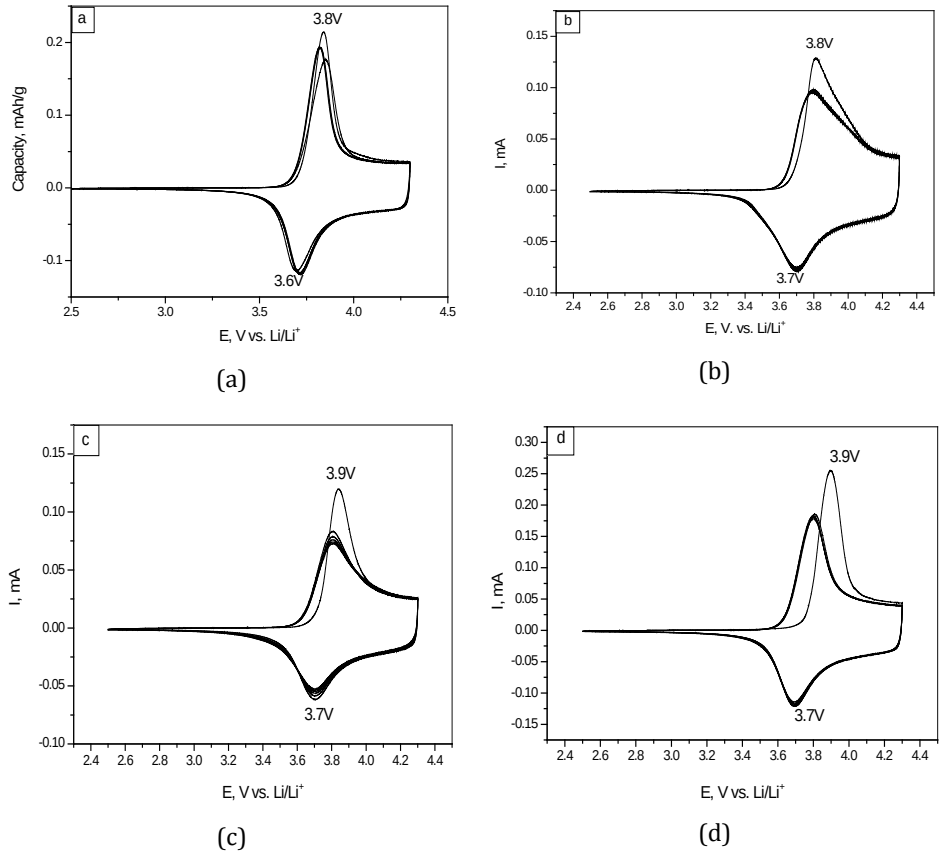

Fig. 9.Cyclic voltammograms of Li//NMC cells using (a) 333SG, (b) 333CP, (c) 333Al, and (d) 333C electrodes at a sweep rate of 0.05 mV s^{-1} between 2.5 and 4.3 V vs. Li^0/Li^+

Figure 10 shows the discharge profile of the four NMC//Li cells. As the rate capability is one of the important electrochemical characteristics of a lithium secondary battery required for high-power storage applications, these measurements were carried out in the voltage range 2.5-4.3V vs. Li0/Li+ at different C-rates i.e. from C/5 to 5C. Slight polarization was observed in the discharge curves of all cells at high C-rates. Since the shape of the discharge profile is similar for the uncoated and coated positive electrodes, it can be

assumed that the Li insertion/extraction mechanism remains unchanged for all NMC materials. Nevertheless, the measured specific capacity at high rates increases for the coated samples, which needs a closer look.

Figure 11 shows the discharge capacities of all four samples as a function of cycle number. It can be seen that the surface modification of NMC particles by alumina (333Al) or carbon (333C) improves the electrochemical behavior leading to a higher capacity for all measured C-rates.

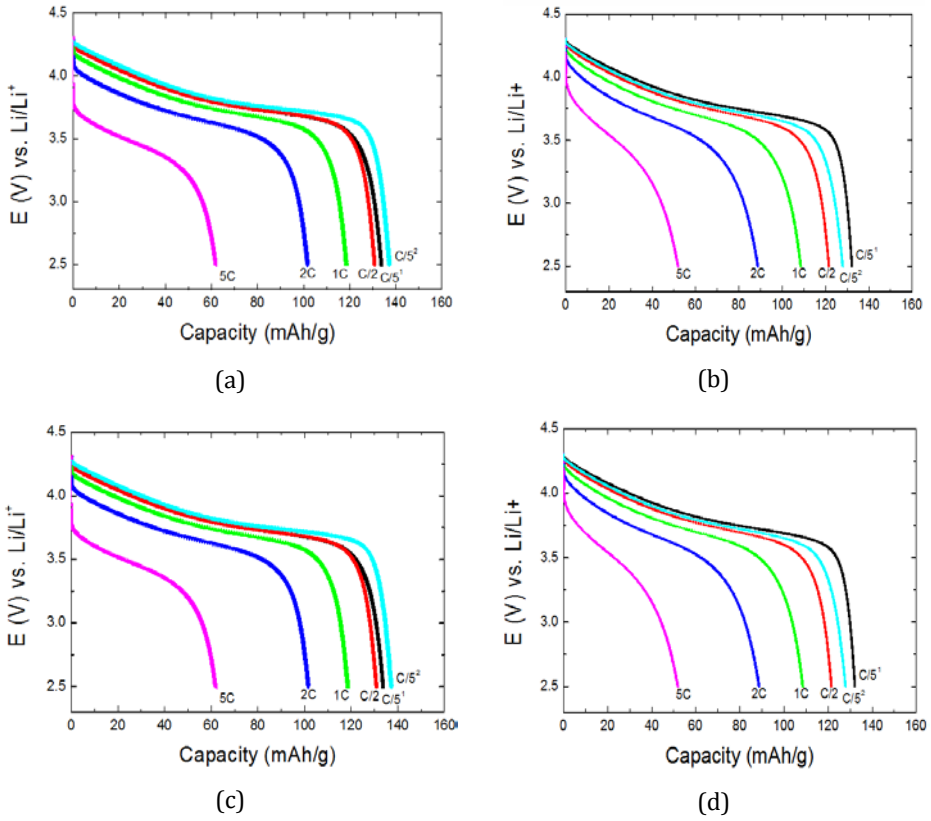

Fig.10.Discharge curves of Li//NMC cells with the samples (a) 333SG, (b) 333CP, (c) 333Al, and (d) 333Cat various C-rates in the potential range 2.5-4.3 V *vs*. Li^0/Li^+

It can also be observed that all samples still have enough flexibility to restore their initial capacities after recovering the low C/5 rate. Figure 12 shows the total discharge capacities as a function of cycle numbers, the upper voltage being 4.5V. The surface modified samples showed a more efficient capacity recovery than the parent cathode material.

Results show the Li/NMC cell with the electrode modified by Al_2O_3 coating displays the highest capacity retention over 50 cycles, which is attributed to the amorphous Al_2O_3 film that impedes the dissolution of transition-metal ions and stabilizes the surface of the positive electrode material [19,47]. However, the specific capacity of this coated NMC electrode decreases significantly in the four first cycles. This is attributed to the insulating nature of Al_2O_3 at the electrode surface that decreases the electrical conductivity of the contact between particles and impedes the transport of the Li ions through the

electrode/electrolyte interface. In the subsequent cycles, the discharge capacity remains stable and shows excellent cycling behavior. The Al_2O_3 layer could be activated by Li ions after several insertion/extraction cycles as reported by Liu et al [48-50].

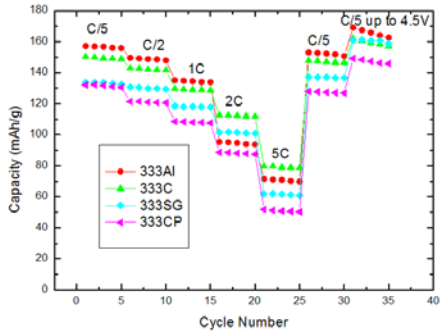

Fig.11. Discharge capacities as a function of cycle number at different C-rates. The potential range was 2.5- 4.3V *vs.*Li^0/Li^+ excepted for the last 5 cycles up to 4.5 V

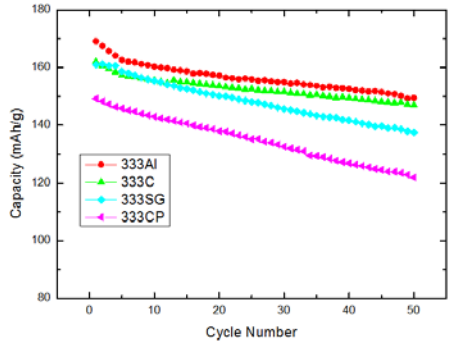

Fig.12. Discharge capacities as a function of cycle number for Li//NMC cells with 333SG, 333CP, 333Al and 333C electrodes carried out in the range 2.5-4.5V after the C-rate test in the potential range 2.5-4.3V.

4. Conclusions

$LiMn_{1/3}Ni_{1/3}Co_{1/3}O_2$ positive electrode materials were prepared by sol-gel and co-precipitation methods. Well-crystallized layered materials with the α-$NaFeO_2$-type structure ($R\bar{3}m$ space group) were obtained for pristine and coated materials as proven using XRD, FTIR and Raman spectroscopy. No influence of the coating on the bulk properties has been revealed. SEM and TEM showed nano-scale particles with a slight tendency to agglomerate and the existence of a thin film encapsulating the NMC particles were identified. Using NMR spectroscopy, significant differences between the sol-gel and the co-precipitation samples have been revealed. Especially, the arrangement of the cations on the transition-metal slabs (intralayer space) is different. It was shown that the transition-metal ions are more randomly distributed in the sol-gel sample compared to the co-precipitation sample.In contrast, no significant difference has been found between the coated and non-coated samples. Nevertheless the appearance of a Li-Al-O phase was revealed for the 333Al sample, which suggests an interface between the NMC bulk and the Al_2O_3-coating layer. The electrochemical tests have shown a significant improvement of

the capacity retention and initial capacity values for the coated NMC positive electrode materials in comparison with uncoated materials.

References

[1] Hong S.A, Nugroho A., Kim S. J., Kim J., Chung K. Y., Cho B-W., Kang J.W. Continuous supercritical hydrothermal synthesis: lithium secondary ion battery applications. Res. Chem. Intermediat. 2011; 37:429–440.http://dx.doi.org/10.1007/s11164-011-0273-3

[2] Ohzuku T.,Makimura Y. Layered Lithium Insertion Material of $LiCo_{1/3}Ni_{1/3}Mn_{1/3}O_2$ for Lithium-Ion Batteries. Chem. Lett .2001; 30:642–643.http://dx.doi.org/10.1246/cl.2001.642

[3] Fey G.T.K., Chang C.S., Kumar T.P. Synthesis and surface treatment of $LiNi_{1/3}Mn_{1/3}Co_{1/3}O_2$ cathode materials for Li-ion batteries. Journal of Solid State Electro .2010; 14: 17-26.http://dx.doi.org/10.1007/s10008-008-0772-3.

[4] Fey G., Chen J.G., Wang Z. F., Yang H. Z., Kumar T. P. Saturated linear dicarboxylic acids as chelating agents for the sol–gel synthesis of $LiNi_{0.8}Co_{0.2}O_2$. Mater. Chem. Phys. 2004; 78: 246-255.

[5] Abdel Ghany A. E., Hashem A. M. A., Abuzeid H. A. M., Eid A. E., Bayoumi H., Julien C. M. Synthesis, structure characterization and magnetic properties of nanosize $LiCo_{1-y}Ni_yO_2$ prepared by sol–gel citric acid route . Ionics. 2009;15: 49-59.http://dx.doi.org/10.1007/s11581-008-0273-5.

[6] Abuzeid H.A.M., Hashem A.M.A., Abdel-Ghany A.E., Eid A.E. , Mauger A., Groult H., Julien C.M. De-intercalation of $LixCo_{0.8}Mn_{0.2}O_2$: A magnetic approach. Journal of Power Sources. 2011; 196: 6440-6448.http://dx.doi.org/10.1016/j.jpowsour.2011.03.054

[7] MacNeil D. D., Lu Z. H.,Dahn J. R. Structure and Electrochemistry of $LiNi_xCo_{1-2x}Mn_xO_2$ ($0<x<1/2$). Journal of Electrochem. Soc. 2002; 149: A1332–A1336.http://dx.doi.org/10.1149/1.1505633.

[8] Liao P. Y., Duh J. G., Sheen S. R. Microstructure and electrochemical performance of LiNi0.6Co0.4−xMnxO2 cathode materials. Journal of Power Sources. 2005; 143: 212–218.http://dx.doi.org/10.1016/j.jpowsour.2004.12.001

[9] Jiangang L., Qian Z., Chao L.,Xiangming H. ZrO2 coating of LiNi1/3Co1/3MnvO2 cathode materials for Li-ion batteries. Ionics. 2009; 15: 493–496.http://dx.doi.org/10.1007/s11581-008-0263-7

[10] Long T., L. Haowen. 2011. Influence of ZnO coating on the structure, morphology and electrochemical performances for $LiNi_{1/3}Mn_{1/3}Co_{1/3}O_2$. Russ. J. Electrochem. 47, 156–160.http://dx.doi.org/10.1134/S1023193511020170

[11] Li D., Kato Y.,Kobayakawa K., Noguchi H., Sato Y. Preparation and electrochemical characteristics of $LiNi_{1/3}Mn_{1/3}Co_{1/3}O_2$ coated with metal oxides coating. Journal of Power Sources. 2006; 160: 1342–1348.http://dx.doi.org/10.1016/j.jpowsour.2006.02.080

[12] Zhang P., Ren X., Yuan Q., Liu J., Zhang Q. Preparation and electrochemical properties of $LiNi_{1/3}Mn_{1/3}Co_{1/3}O_2$ –PPy composites cathode materials for lithium-ion battery. Synth. Met. 2011; 161: 1092–1097.http://dx.doi.org/10.1016/j.synthmet.2011.03.021

[13] Sathiya M., Prakash A.S., Ramesha K., Shukla A.K. Rapid synthetic routes to prepare $LiNi_{1/3}Mn_{1/3}Co_{1/3}O_2$ as a high voltage, high-capacity Li-ion battery cathode material. Materials Research Bull. 2009; 44: 1990–1994.http://dx.doi.org/10.1016/j.materresbull.2009.06.007

[14] Sinh N.N., Munichandraiah N. Synthesis and characterization of carbon-coated $LiNi_{1/3}Mn_{1/3}Co_{1/3}O_2$ in a single step by an inverse microemulsion route. ACS. Appl. Mater. Interfaces. 2009; 1:1241–9.http://dx.doi.org/10.1021/am900120s

[15] Singh G., Sil A., Ghosh S., Panwar A. Effect of citric acid content on synthesis of $LiNi_{1/3}Mn_{1/3}Co_{1/3}O_2$ and its electrochemical characteristics. Ceram. Int. 2010; 36: 1831–1836.http://dx.doi.org/10.1016/j.ceramint.2010.03.028

[16] Hashem A. M. A., Abdel-Ghany A. E. , Eid A. E., Trottier J., Zaghib K. , Mauger A., Julien C. M. Study of the surface modification of LiNi1/3Co1/3Mn1/3O2 cathode material for lithium ion battery. Journal of Power Sources. 2011; 196: 8632–8637.http://dx.doi.org/10.1016/j.jpowsour.2011.06.039

[17] Wang M., Wu F., Su Y., Chen S. Modification of $LiCo_{1/3}Ni_{1/3}Mn_{1/3}O_2$ cathode material by CeO_2-coating. Science in China Series E: Technological Sciences. 2009; 52:2737–2741.http://dx.doi.org/10.1007/s11431-008-0306-3

[18] Li J., Fan M., He X., Zhao R., Jiange C., Wan C. TiO2 coating of $LiNi_{1/3}Mn_{1/3}Co_{1/3}O_2$ cathode materials for Li-ion batteries. Ionics. 2006; 12: 215–218.http://dx.doi.org/10.1007/s11581-006-0034-2

[19] Peng Z. , Deng X. , Du K. , Hu G., Gao X. , Liu Y. Coating of $LiNi_{1/3}Mn_{1/3}Co_{1/3}O_2$ cathode materials with alumina by solid state reaction at room temperature. Journal of Central South University of Technology. 2008; 15: 34–38.http://dx.doi.org/10.1007/s11771-008-0008-9

[20] Huang Y., Chen J., Ni J., Zhou H., Zhang X. A modified ZrO_2-coating process to improve electrochemical performance of $Li(Ni_{1/3}Co_{1/3}Mn_{1/3})O_2$. Journal of Power Sources. 2009; 188:538–545.http://dx.doi.org/10.1016/j.jpowsour.2008.12.037

[21] Guo R., Shi P., Cheng X., Ma Y.,Tan Z. Effect of Ag additive on the performance of $LiNi_{1/3}Mn_{1/3}Co_{1/3}O_2$ cathode material for lithium ion battery. Journal of Power Sources. 2009; 189: 2–8.http://dx.doi.org/10.1016/j.jpowsour.2009.01.016

[22] Riley L.A., Van Atta S., Cavanagh A.S, Yan Y., George S. M., Liu P., Dillon A. C., Lee S.-H. Electrochemical effects of ALD surface modification on combustion synthesized $LiNi_{1/3}Mn_{1/3}Co_{1/3}O_2$ as a layered-cathode materia. Journal of Power Sources. 2011; 196: 3317–3324. http://dx.doi.org/10.1016/j.jpowsour.2010.11.124

[23] Myung S.T., Izumi K., Komaba S., Sun Y.-K., Yashiro H.,Kumagai N. Role of alumina coating on Li–Ni–Co–Mn–O particles as positive electrode material for lithium-ion batteries. Chem. Mater., 2005; 17:3695-3704.http://dx.doi.org/10.1021/cm050566s

[24] Rougier A., Gravereau P.,Delmas C. Optimization of the composition of the $Li_{1-z}Ni_{1+z}O_2$ electrode material: structural, magnetic, and electrochemical studies. Journal of Electrochem. Soc.1996; 143:1168–1175.http://dx.doi.org/10.1149/1.1836614

[25] Luo X., Wang X. X., Liao L., Gamboa S., Sebastian P.J. Effects of synthesis conditions on the structural and electrochemical properties of layered $Li[Ni_{1/3}Co_{1/3}Mn_{1/3}]O_2$ cathode material via the hydroxide co-precipitation method LIB SCITECH. Journal of Power Sources. 2006;158: 601–605.http://dx.doi.org/10.1016/j.jpowsour.2006.03.090

[26] Yoon W.S., Grey C. P., Balasubramanian M., Yang X.-Q., Fischer D. A., McBreen J.Combined NMR and XAS study on local environments and electronic structures of electrochemically Li-ion deintercalated $Li_{1-x}Co_{1/3}Ni_{1/3}Mn_{1/3}O_2$ electrode system. Electrochem. Solid-State. Lett. 2004; 7: A53 http://dx.doi.org/10.1149/1.1643592

[27] Cahill L. S., Yin S.C., Samoson A., Heinma I., Nazar L. F.,Goward G. R. 6Li NMR studies of cation disorder and transition metal ordering in $Li[Ni_{1/3}Co_{1/3}Mn_{1/3}]O_2$ using ultrafast magic angle Spinning. Chem. Mater. 2005; 17: 6560–6566.http://dx.doi.org/10.1021/cm0508773

[28] Zeng D., Cabana J., Bréger J., Yoon W.S., Grey C. P. Cation ordering in $Li[Ni_xMn_xCo_{(1-2x)}]O_2$ -layered cathode materials: A nuclear magnetic resonance (NMR), pair distribution function, X-ray absorption spectroscopy, and electrochemical study.Chem. Mater. 2007; 19: 6277–6289 http://dx.doi.org/10.1021/cm702241a

[29]Yabuuchi N., Ohzuku T. Novel lithium insertion material of $LiCo_{1/3}Ni_{1/3}Mn_{1/3}O_2$ for advanced lithium-ion batteries. Journal of Power Sources. 2003; 119-121: 171–174

http://dx.doi.org/10.1016/S0378-7753(03)00173-3
[30] Wang H.,Tang A., Huang K., Liu S. Uniform AlF3 thin layer to improve rate capability of $LiNi_{1/3}Mn_{1/3}Co_{1/3}O_2$ material for Li-ion batteries. Transactions of Nonferrous Metals Society of China. 2010; 20:803–808 http://dx.doi.org/10.1016/S1003-6326(09)60217-X
[31] Wu H. M., Belharouak I., Abouimrane A., Sun Y.-K., Amine K. Surface modification of $LiNi_{0.5}Mn_{1.5}O_4$ by ZrP_2O_7 and ZrO_2 for lithium-ion batteries. Journal of Power Sources. 2010; 195: 2909–2913 http://dx.doi.org/10.1016/j.jpowsour.2009.11.029
[32] Julien C., Massot M. Raman scattering of $LiNi_{1-y}Al_yO_2$. Solid State Ionics. 2002; 148: 53–59 http://dx.doi.org/10.1016/S0167-2738(02)00117-0
[33] Julien C., Letranchant C., Rangan S., Lemal M., Ziolkiewicz S., Castro-Garci S., El-Farh L., Benkaddour M. Layered $LiNi_{0.5}Co_{0.5}O_2$ cathode materials grown by soft-chemistry via various solution methods. Materials Science and Engineering: B. 2000; 76:145–155 http://dx.doi.org/10.1016/S0921-5107(00)00431-1
[34] Julien C. Local cationic environment in lithium nickel–cobalt oxides used as cathode materials for lithium batteries. Solid State Ionics. 2000; 136-137: 887–896.http://dx.doi.org/10.1016/S0167-2738(00)00503-8
[35] Kosova N. V., Devyatkina E. T. Comparative study of $LiCoO_2$ surface modified with different oxides. Journal of Power Sources. 2007; 174: 959–964.http://dx.doi.org/10.1016/j.jpowsour.2007.06.129
[36] Mackenzie K., Smith M. E. Multinuclear Solid-State NMR of Inorganic Materials. Elsevier (Pergamon Materials Series)Oxford.2002; 6.
[37] Duer M. J. Introduction to Solid-State NMR Spectroscopy. Blackwell Publishing: Oxford. 2004.
[38] Indris S., Cabana J., Rutt O. J., Clarke S. J., Grey C. P. Layered oxysulfides $Sr_2MnO_2Cu_2m_{0.5}Sm_{+1}$ (m = 1, 2, and 3) as insertion hosts for Li ion batteries. Journal of Am. Chem. Soc. 2006; 128, 13354.http://dx.doi.org/10.1021/ja064961a
[39] Grey C. P., Dupré N. NMR Studies of cathode materials for lithium-ion rechargeable batteries. Chemical Reviews. 2004; 104:4493–4512.http://dx.doi.org/10.1021/cr020734p
[40] Ménétrier M., Bains J., Croguennec L., Flambard A., Bekaert E., Jordy C., Biensan P., Delmas C. NMR evidence of LiF coating rather than fluorine substitution in $Li(Ni_{0.425}Mn_{0.425}Co_{0.15})O_2$. Journal of Solid State Chemistry. 2008; 181:3303–3307.http://dx.doi.org/10.1016/j.jssc.2008.09.002
[41] Cherkashinin G., Nikolowski K., Ehrenberg H., Jacke S., Dimesso L., Jaegermann W. The stability of the SEI layer, surface composition and the oxidation state of transition metals at the electrolyte–cathode interface impacted by the electrochemical cycling: X-ray photoelectron spectroscopy investigation. Physical Chemistry. 2012;14: 12321–12331.http://dx.doi.org/10.1039/c2cp41134b
[42] Dupré N., Martin J.-F., Guyomard D., Yamada A.,Kanno R. Characterization of interphases appearing on $LiNi_{0.5}Mn_{0.5}O_2$ using ^7Li MAS NMR. Journal of Power Sources. 2009; 189: 557–560.http://dx.doi.org/10.1016/j.jpowsour.2008.10.017
[43] Chernova N. A., Ma M., Xiao J., Whittingham M. S., Breger J., Grey C. P. Layered $Li_xNi_yMn_yCo_{1-2y}O_2$ Cathodes for Lithium Ion Batteries: Understanding Local Structure via Magnetic Properties. Chem. Mater. 2007; 19: 4682–4693.http://dx.doi.org/10.1021/cm0708867
[44] Shaju K., Subba Rao G. V., Chowdari B.V.R. Performance of layered $Li(Ni_{1/3}Co_{1/3}Mn_{1/3})O_2$ as cathode for Li-ion batteries. Electrochim. Acta. 2002; 48: 145–151.http://dx.doi.org/10.1016/S0013-4686(02)00593-5
[45] Chen Z., Dahn J. R. Methods to obtain excellent capacity retention in $LiCoO_2$ cycled to 4.5 V. Electrochim. Acta. 2004; 49:1079–1090.http://dx.doi.org/10.1016/j.electacta.2003.10.019

[46] Zhang X., Mauger A., Lu Q., Groult H., Perrigaud L., Gendron F., Julien C. M. Synthesis and characterization of $LiNi_{1/3}Mn_{1/3}Co_{1/3}O_2$ by wet-chemical method. Electrochim. Acta. 2010; 55: 6440–6449.http://dx.doi.org/10.1016/j.electacta.2010.06.040

[47] Zheng J. M., Li J., Zhang Z. R., Guo X. J., Yang Y. The effects of TiO2 coating on the electrochemical performance of $Li[Li_{0.2}Mn_{0.54}Ni_{0.13}Co_{0.13}]O_2$ cathode material for lithium-ion battery. Solid State Ionics. 2008; 179: 1794–1799.http://dx.doi.org/10.1016/j.ssi.2008.01.091

[48] Liu L., Wang Z., Li H., Chen L., Huang X. Al_2O_3-coated $LiCoO_2$ as cathode material for lithium ion batteries. Solid State Ionics. 2002;152-153:341-346.http://dx.doi.org/10.1016/S0167-2738(02)00333-8

[49] Kazuhiro A., Noboru T., Hikari S., Kuniaki T., Zempachi O. Electrochemical properties of $LiNi_{1/3}Mn_{1/3}Co_{1/3}O_2$ cathode material modified by coating with Al_2O_3 nanoparticles. Journal of Power Sources. 2014:269: 236-243.http://dx.doi.org/10.1016/j.jpowsour.2014.06.101

[50] Qi Q.,Xi H.,Yanmei C.,YanT.,Weizhong L. Al_2O_3 coated $LiNi_{1/3}Mn_{1/3}Co_{1/3}O_2$ cathode material by sol–gel method: Preparation and characterization. Ceramics International. 2014: 40: 10511–10516.http://dx.doi.org/10.1016/j.ceramint.2014.03.023